RESEARCH ARTICLE

A partition-type tubular scaffold loaded with PDGF-releasing microspheres for spinal cord repair facilitates the directional migration and growth of cells

Xue Chen[1, 2, 3], Mei-Ling Xu[2], Cheng-Niu Wang[2], Lu-Zhong Zhang[4], Ya-Hong Zhao[4], Chang-Lai Zhu[4], Ying Chen[2], Jian Wu[2], Yu-Min Yang[4], Xiao-Dong Wang[2, *]

1 School of Biology & Basic Medical Sciences, Soochow University, Suzhou, Jiangsu Province, China
2 Department of Histology and Embryology, Medical College, Nantong University, Nantong, Jiangsu Province, China
3 Wuxi School of Medicine, Jiangnan University, Wuxi, Jiangsu Province, China
4 Jiangsu Key Laboratory of Neuroregeneration, Co-innovation Center of Neuroregeneration, Nantong University, Nantong, Jiangsu Province, China

Funding: *This study was supported by the Natural Science Foundation of China, No. 81501610, 81350030; the Priority Academic Program Development of Jiangsu Higher Education Institutes of China.*

Graphical Abstract

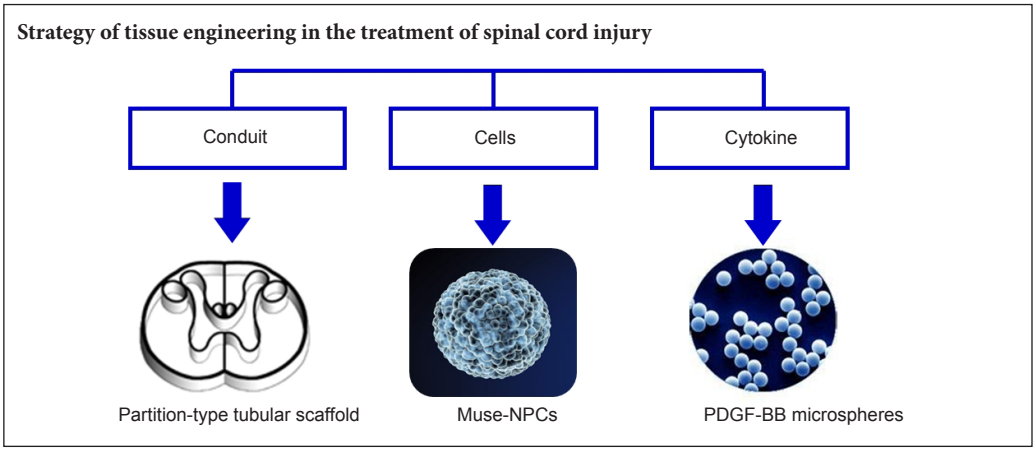

***Correspondence to:**
Xiao-Dong Wang, M.D., wxdzw@ntu.edu.cn.

orcid:
0000-0003-4813-6858 (Xiao-Dong Wang)

doi: *10.4103/1673-5374.235061*

Accepted: *2018-04-15*

Abstract

The best tissue-engineered spinal cord grafts not only match the structural characteristics of the spinal cord but also allow the seed cells to grow and function *in situ*. Platelet-derived growth factor (PDGF) has been shown to promote the migration of bone marrow stromal cells; however, cytokines need to be released at a steady rate to maintain a stable concentration in vivo. Therefore, new methods are needed to maintain an optimal concentration of cytokines over an extended period of time to effectively promote seed cell localization, proliferation and differentiation. In the present study, a partition-type tubular scaffold matching the anatomical features of the thoracic 8–10 spinal cord of the rat was fabricated using chitosan and then subsequently loaded with chitosan-encapsulated PDGF-BB microspheres (PDGF-MSs). The PDGF-MS-containing scaffold was then examined *in vitro* for sustained-release capacity, biocompatibility, and its effect on neural progenitor cells differentiated *in vitro* from multilineage-differentiating stress-enduring cells (MUSE-NPCs). We found that pre-freezing for 2 hours at −20°C significantly increased the yield of partition-type tubular scaffolds, and 30 μL of 25% glutaraldehyde ensured optimal crosslinking of PDGF-MSs. The resulting PDGF-MSs cumulatively released 52% of the PDGF-BB at 4 weeks *in vitro* without burst release. The PDGF-MS-containing tubular scaffold showed suitable biocompatibility towards MUSE-NPCs and could promote the directional migration and growth of these cells. These findings indicate that the combination of a partition-type tubular scaffold, PDGF-MSs and MUSE-NPCs may be a promising model for the fabrication of tissue-engineered spinal cord grafts.

Key Words: *nerve regeneration; partition-type tubular scaffold; microspheres; platelet-derived growth factor; muse cells; neural precursor cells; chitosan; encapsulation efficiency; bone marrow; spinal cord injury; tissue engineering; neural regeneration*

Introduction

Spinal cord injuries (SCIs) are increasingly common in emergency medicine. SCI patients often suffer from limb disorders and life-long paralysis (Ahuja et al., 2017; Kornhaber et al., 2017). At present, the major clinical strategy is to reduce secondary injury; however, it has little impact on functional recovery. Therefore, there is an urgent need for new effective treatment methods, in which tissue engineering probably has the greatest potential (Kim and Lee, 2014; Agbay et al., 2016; Muheremu et al., 2016; Wang, 2018).

Design and production of the scaffold is the first major task of tissue engineering. In previous studies on defect-type SCI repair, many configurations of bridging scaffolds were used, such as single tubes, multiple channels, numerous

microchannels, and porous cylinders (Bellamkonda, 2006; Bryant et al., 2007; Madigan et al., 2009). These designs were mainly for repairing peripheral nerve defects. Because the peripheral nerve is a cable-type structure, these configurations can meet the requirements of peripheral nerve repair. However, in contrast, the spinal cord contains both gray matter and white matter. The gray matter is where neuronal cell bodies concentrate, while the white matter contains multiple ascending and descending fiber bundles.

Because of the complex structure of the spinal cord, the effectiveness of repair is greatly impacted by the scaffold design. Therefore, we designed a partition-type tubular scaffold that can partition the gray matter from the white matter according to the histological structure of the spinal cord. A chitosan scaffold matching the white matter corticospinal and rubrospinal tracts has been shown to satisfactorily repair the injured rat spinal cord (Wang et al., 2013).

Another key element of tissue-engineered scaffolds is seed cells. Currently, widely used seed cells for neuronal repair include neural stem and progenitor cells (NSCs or NPCs), oligodendrocyte precursor cells, olfactory ensheathing cells, mesenchymal stem cells (MSCs) and Schwann cells. Bone marrow is the original source of MSCs. Bone marrow stromal cells (BMSCs) have become a hot topic of research because of their convenient harvesting and strong differentiation potential (Jia et al., 2012; Zhang et al., 2016). However, the composition of BMSCs is complex, and the differentiation abilities of the various cell types are quite different (Hong et al., 2014; Lu et al., 2014; Kawabata et al., 2016; Nagoshi and Okano, 2017). Only a small percentage of cells have the potential for broad differentiation, such as multilineage-differentiating stress-enduring (muse) cells (Kuroda et al., 2010; Tetzlaff et al., 2011; Wright et al., 2011; Hoffman et al., 2016; Badner et al., 2017). The newly discovered pluripotent stem cell may be an ideal candidate seed cell.

The amount of implanted seed cells is limited, and these cells can migrate *in vivo*. Therefore, only a few cells are actually available at the transplant site (Assinck et al., 2017). This will inevitably reduce the usefulness of seed cells (Assinck et al., 2017).

A major objective of tissue engineering is to enhance the effectiveness of seed cells at the transplant site. A previous study found that platelet-derived growth factor-BB (PDGF-BB) has a chemotactic effect towards BMSCs (Ponte et al., 2007). This requires that PDGF-BB is continually maintained at an active concentration and attracts seed cells to the transplant site for a relatively long period.

In the present study, microspheres (MSs) were used to maintain sustained release of protein/peptide drugs (Mohtaram et al., 2013; Ma, 2014; Pascual-Gil et al., 2015). Chitosan-encapsulated PDGF-BB microspheres (PDGF-MSs) were fabricated and incorporated into the partition-type tubular scaffold to support the growth and functioning of muse cells. Electron microscopy, cell culture, immunohistochemistry and cell viability assay were conducted to characterize the biocompatibility and biological action of the partition-type tubular scaffold loaded with PDGF-MSs *in vitro*.

Materials and Methods

Preparation of the partition-type tubular scaffold

Molds for the partition-type tubular scaffold were designed and made based on immunohistochemistry of T_{8-10} segments, the gray matter, white matter, corticospinal tract and rubrospinal tract of Sprague-Dawley rats weighing 180–220 g (Wang et al., 2013).

The chitosan partition-type tubular scaffold was prepared using the freeze-drying method (China Patent: ZL200810100637.2). For this process, 0.45 g chitosan (Nantong Xincheng Biochemical Company, Jiangsu, China) was dissolved in 8 mL 2% acetic acid solution and mixed with 2 mL 10% aqueous gelatin solution (Sigma-Aldrich, St. Louis, MO, USA). Then, 0.45 g chitin (Nantong Xincheng Biochemical Company) was added, heated and mixed to prepare the chitosan-chitin solution. The chitosan-chitin solution (400 μL) was absorbed and injected into the mold at −20°C for 2.5 hours. After removal of the outer part of the mold, the chitosan partition-type tubular scaffold with the mold core was neutralized in 10% NaOH (Shanghai Ling Feng Chemical Reagents Company, Shanghai, China) for 2 hours. The scaffold was washed with ultrapure water until the pH was neutral. The partition-type tubular scaffold was then placed in freeze-drying bottles. Four groups of scaffolds were then subjected to pre-freezing at −20°C for 1, 2, 3 or 4 hours, and then frozen and dried at −40°C and 0.02 Pa for 1 hour using a freeze dryer (Labconco, Kansas City, MO, USA). After removal of the mold core, the partition-type tubular scaffold was exposed to Co60 irradiation for disinfection, and then sealed and preserved for further use.

Preparation of MSs

MSs were prepared by an emulsification method using glutaraldehyde (Sigma-Aldrich) as crosslinker (Jiang et al., 2014). Chitosan, 0.025 g, was dissolved in 1 mL 2% acetic acid solution overnight. Span 80 (Sigma-Aldrich), 0.2 mL, was added to a flask containing 9.8 mL liquid paraffin and stirred at 500 r/min for 30 minutes, forming an oil phase. Then, 1 mL of the aqueous phase was added to the oil phase, followed by stirring at 500 r/min for 30 minutes, forming an emulsion. Glutaraldehyde, 25%, was slowly added and stirred at 1500 r/min for 1 hour. To determine the optimal conditions for the preparation of MSs, four groups were established, with glutaraldehyde volumes of 10, 20, 30 and 40 μL. The mixture was centrifuged at 200 × *g* for 5 minutes. After removal of the supernatant, the samples were washed twice with 30 mL petroleum ether (Shanghai Ling Feng Chemical Reagents Company), 25 mL isopropanol (Sigma-Aldrich) and 20 mL acetone (Shanghai Ling Feng Chemical Reagents Company) separately by shaking. The samples were then centrifuged at 200 × *g* for 10 minutes, kept without agitation for 5 minutes, and the supernatant was discarded. The precipitate was dried at room temperature. MSs were collected and stored at room temperature.

Determination of MS diameter

The prepared MSs were randomly adhered to double-sided

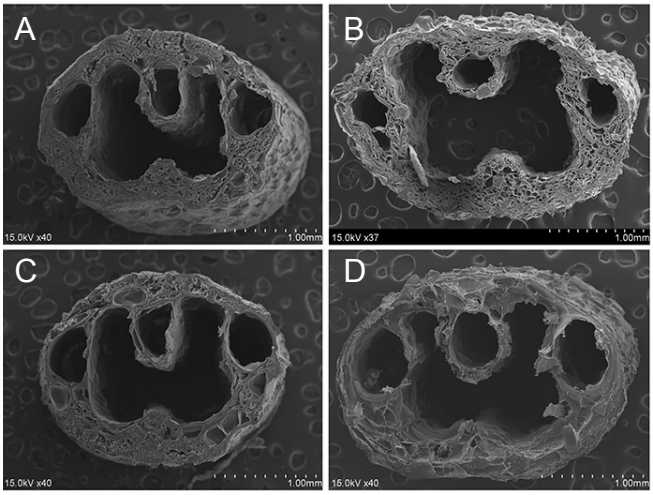

Figure 1 Scanning electron microscopy of a cross section of the partition-type tubular scaffold at various freezing time points.
(A) 1-hour group; (B) 2-hour group; (C) 3-hour group; (D) 4-hour group. The porosity of the partition-type tubular scaffold was higher in the 2-hour group than in the other groups. Scale bars: 1.0 mm.

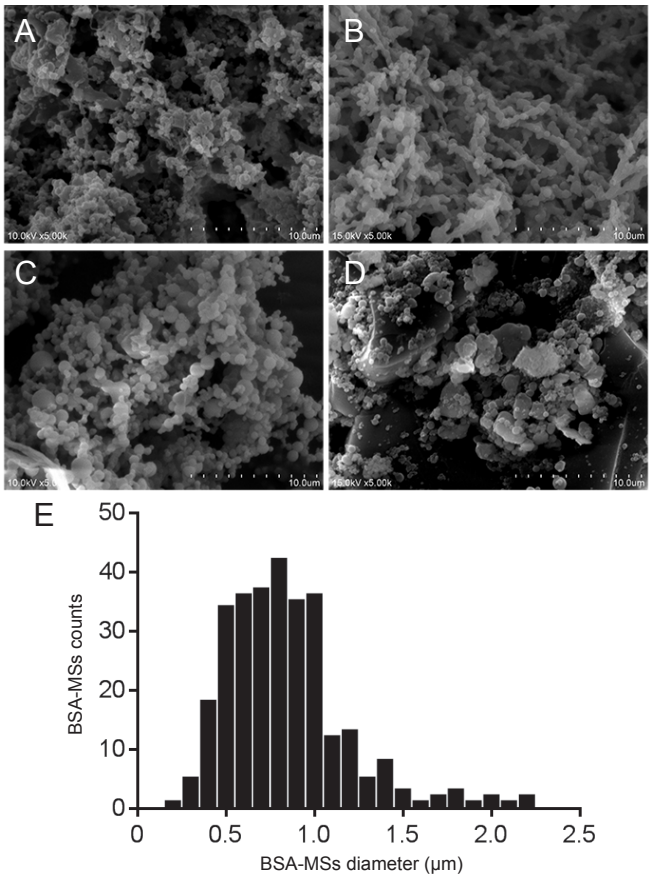

Figure 2 Scanning electron microscopy of MSs prepared using different amounts of glutaraldehyde.
A 30 μL volume of 25% glutaraldehyde was optimal for preparing MSs. (A) 10 μL group; (B) 20 μL group; (C) 30 μL group; (D) 40 μL group. Scale bars: 10 μm. (E) MS diameter in the 30 μL group. All experiments were conducted six times. MSs: Microspheres; BSA: bovine serum albumin.

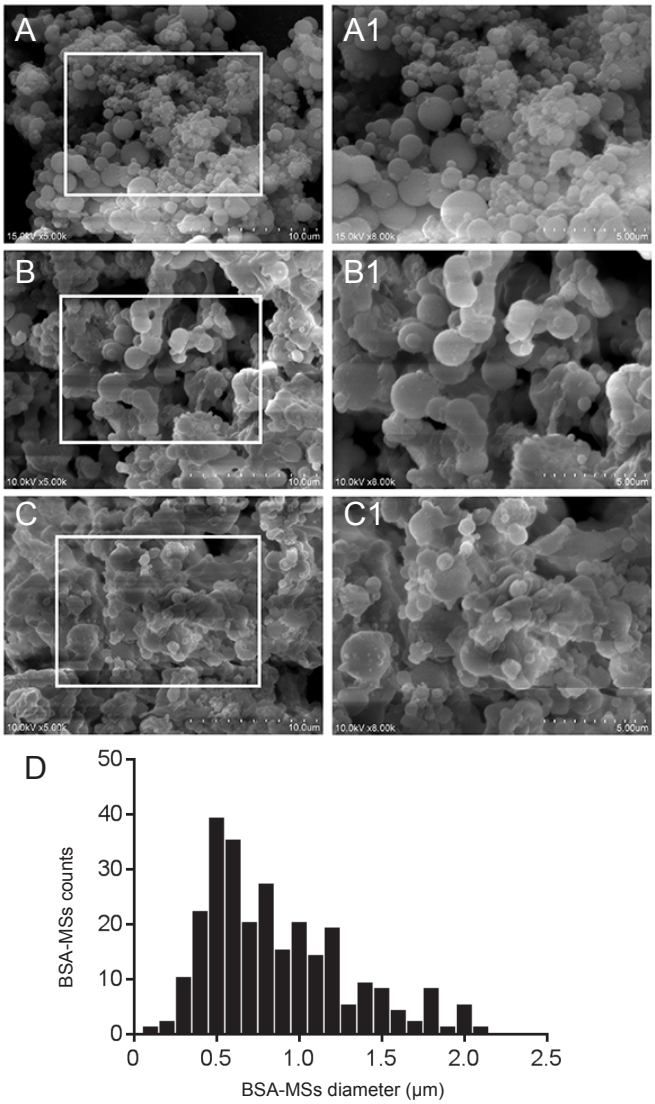

Figure 3 Scanning electron microscopy of MSs encapsulated with different amounts of BSA.
With 1 mg BSA, MS molding was good. (A) 1 mg group; (B) 2 mg group; (C) 4 mg group. (A1–C1) Magnified views of the boxed areas in A–C, respectively. Scale bars: 10 μm (A–C) and 5.0 μm (A1–C1). (D) BSA-MS diameter in the 1 mg group. All experiments were conducted six times. MSs: Microspheres; BSA: bovine serum albumin.

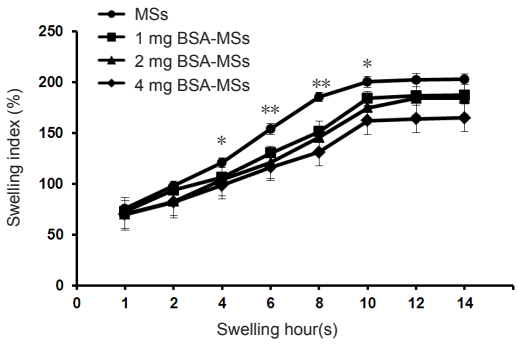

Figure 4 Swelling index of MSs.
Compared with the MSs group, the swelling index was lower in the three BSA encapsulation groups. Swelling index of MSs gradually decreased as the amount of BSA increased. $*P < 0.05$, $**P < 0.01$, *vs.* 1, 2 and 4 mg BSA-MSs groups (mean ± SD; two-way analysis of variance followed by Dunnett's *post hoc* test). All experiments were conducted six times. MSs: Microspheres; BSA: bovine serum albumin.

tape on the specimen holder of a scanning electron microscope (SEM) (S-3400; Hitachi, Tokyo, Japan) and coated with gold using an auto fine coater (JFC-1600; JEOL, Tokyo, Japan). The diameters of the MSs in the different groups were evaluated under the SEM.

Determination of MS swelling index

Dry MSs (W_d), 10 mg, were added to 1 mL of ultrapure water and shaken on a shaker (Kylin-Bell Lab Instruments Co., Ltd, Jiangsu, China) at 100 r/min for 1, 2, 4, 6, 8, 10, 12 or 14 hours, followed by centrifugation (Thermo Fisher, Waltham, MA, USA) at 400 × *g* for 5 minutes. The supernatant was discarded. After excess water on the surface of the MSs was absorbed with filter paper, the sample was immediately weighed (W_s). The swelling index (%) was calculated with the following formula: $[(W_s-W_d)/W_d] \times 100\%$.

Preparation and observation of partition-type tubular scaffolds containing MSs

MSs, 60 mg, were resuspended in 200 μL ultrapure water. This suspension was then injected gradually, from the inside to the outside, at both ends of the gray matter tube of the partition-type tubular scaffold. Thus, the suspension was evenly distributed in the tube. The MS-containing partition-type tubular scaffold was frozen and dried with the freeze dryer, and then, the surface was coated with gold and observed with a scanning electron microscope (Hitachi).

Bovine serum albumin (BSA)-MS preparation

To evaluate the encapsulation efficiency of the MSs for protein, BSA was selected as the model protein. Three BSA (Biosharp, Anhui, China) groups were established—1, 2 and 4 mg. BSA was added to 1 mL of the aqueous phase of a 2.5% chitosan solution. Subsequently, the aqueous phase was slowly added to 10 mL of the oil phase, forming an emulsion by stirring at 500 r/min for 30 minutes. The subsequent steps are identical to those for the preparation of the MSs.

Determination of BSA encapsulation efficiency

Petroleum ether, isopropanol and acetone eluent in the preparation of BSA-MSs were centrifuged at 200 × *g* for 10 minutes. After removal of the supernatant, the residue was air-dried and dissolved in 200 μL ultrapure water. Then, using a 20-μL aliquot of this solution, the optical density was measured at 595 nm using the BCA enhancement kit to estimate protein concentration (Beyotime, Jiangsu, China). BSA weight (W_{BSA}) in the eluent was calculated. Using the weight of the BSA added initially, encapsulation efficiency (%) was calculated as: $[(W_{initial}-W_{BSA})/W_{initial}] \times 100\%$.

BSA release study

BSA-MSs, 30 mg, were resuspended in 6 mL of pH 7.4 phosphate-buffered saline (PBS), and shaken on a horizontal shaker (Kylin-Bell) at 60 r/min and room temperature. The supernatant, 200 μL, was collected at 1, 3, 5, 7, 9, 11, 14, 21 and 28 days, and stored at −20°C. The BSA concentration in the supernatant was measured at various time points with a BSA ELISA kit (RapidBio, Shanghai, China). Standards and blank controls (same volume of PBS) were made for each time point. Each group contained three replicate wells. Optical density values were measured at 450 nm with a microplate reader (Bio-Tek, Winooski, VT, USA). Cumulative release was calculated based on the standard curve.

PDGF-MS preparation

PDGF-BB (PeproTech, Jiangsu, China), 1 μg, was added to 1 mL of the aqueous phase of a 2.5% chitosan solution, which was then gradually added to the oil phase to form an emulsion. The other steps were identical to those for the preparation of BSA-MSs. The sustained release curve for the PDGF-MSs was then determined.

MUSE-NPC preparation and assessment

Bone marrow samples were provided by the Department of Hematology, Affiliated Hospital of Nantong University, China, after obtaining informed consent and approval by the School Ethics Committee of Affiliated Hospital of Nantong University (No. 2015-052).

Human BMSCs were isolated as described by our group previously (5 cases, males, average age of 40 years) (Wang et al., 2016). Briefly, 2–3 mL of healthy adult bone marrow was separated by Histopaque-1077 (Sigma-Aldrich) density gradient centrifugation and the differential adhesion method to harvest BMSCs. To isolate muse cells based on their resistance to stress, the cells were treated with 0.25% trypsin-EDTA (Thermo Fisher) and routinely cultured for 8 hours. Trypsinization was terminated by adding fetal bovine serum (Thermo Fisher). The cells were resuspended and shaken with a vortex device (Kylin-Bell) at 2000 r/min for 3 minutes, and thereafter seeded onto poly-HEMA-coated 12-well plates with 0.9% MC medium (Stemcell, Shanghai, China). Then, 3–5 days later, muse cell spheres formed. After proliferation and passage, cells at 1×10^5/mL were seeded in MEM medium (Thermo Fisher) containing 20% fetal bovine serum. MUSE cells proliferated and were subcultured using the alternating suspension–adhesion culture method. The MUSE cell spheres were then harvested and triturated into single cells. These single cells were cultured in neural induction medium (DMEM/F12 (Thermo Fisher) supplemented with 20 ng/mL epidermal growth factor (Sigma-Aldrich), 20 ng/mL basic fibroblast growth factor (Sigma-Aldrich) and 1% B27 (Thermo Fisher)). The differentiated cell spheres were subjected to immunocytochemical staining using the DCX-FITC antibody (1:50; BD, San Diego, CA, USA).

Evaluation of the effects of the MS/partition-type tubular scaffold on MUSE-NPC growth

MSs, 50 mg, and the partition-type tubular scaffold, 500 mg, were immersed in 10 mL neural induction medium for 48 hours to prepare MS and partition-type tubular scaffold leachates. MUSE-NPCs, 200 μL, at 2.5×10^4/mL, were cultured in precoated 96-well plates containing the leachates for 1, 3, 5 or 7 days. Nerve induction medium alone was used as a control group. Each group contained six parallel

replicate wells. Cell viability was measured with a CCK-8 kit (Beyotime).

MS/partition-type tubular scaffold, 10 mg, was cultured with MUSE-NPCs. MUSE-NPCs, 200 μL, at 5×10^4/mL, were seeded on the scaffold in 12-well plates. Each well contained 1 mL neural induction medium. The time points and control group were the same as those for the leachate test. Cell growth was observed using a microscope (IX70; Olympus, Tokyo, Japan).

Assessment of the effects of PDGF-BB on MUSE-NPC growth

MUSE-NPCs, 200 μL, at 1×10^5/mL, were incubated in polylysine-coated 48-well plates. Each well contained 100 μL neural induction medium and 0, 30, 60, 90 or 120 ng/mL PDGF-BB. After 1, 3, 5 and 7 days of culture, cell growth was observed using the microscope. Cell proliferation rate was determined with the CCK-8 kit (Beyotime). Cells were cultured with 120 ng/mL PDGF-BB for 7 days, subjected to immunocytochemical staining using rabbit anti-MAP-2 antibody (1:1000; Millipore, CA, USA) and FITC-labeled goat anti-rabbit IgG antibody (1:500; Sigma-Aldrich), and observed by fluorescence microscopy (TCS SP8; Leica, Wetzlar, Germany).

MUSE-NPCs, 200 μL, at 1×10^4/mL, were seeded in the upper chamber of a 6.5 mm Transwell (pore size: 8.0 μm; Corning, NY, USA). Neural induction medium, 500 μL, containing 0 or 120 ng/mL PDGF-BB, was added to the lower chamber. After 12 hours of culture, the membrane was stained with crystal violet. Four fields were randomly selected, and cells traversing to the lower chamber were quantified and analyzed with the light microscope (IX70; Olympus). For another experiment, 200 μL of a MUSE-NPC cell suspension, 1×10^4/mL, was seeded into culture wells containing 10 mg of partition-type tubular scaffold and PDGF-MSs along with 120 ng/mL PDGF-BB and cultured for 1 month.

Statistical analysis

Data were expressed as the mean ± SD and analyzed using GraphPad Prism 6.0 software (GraphPad Software Inc., La Jolla, CA, USA). All experiments were conducted six times. Experimental data were analyzed with one-way or two-way analysis of variance, followed by Dunnett's *post hoc* test. A value of $P < 0.05$ was considered statistically significant.

Results

Observation of the partition-type tubular scaffold

The duration of pre-freezing at −20°C affected the scaffold molding rate and porosity. Of the four time points tested, the molding rate was substantially higher in the 2-hour group (approximately 69%) than in the other groups. Under the SEM, the porosity of the partition-type tubular scaffold was higher in the 2-hour group than in the other groups (**Figure 1**). Therefore, 2 hours was selected as the optimal pre-freezing time for the preparation of the partition-type tubular scaffold.

MS observation and evaluation

MS diameter

The use of the crosslinker glutaraldehyde leads to changes in the morphology and diameter of MSs (Ma et al., 2014). With all four concentrations of glutaraldehyde, the MSs displayed a spherical structure. However, the sphere-forming rate was highest only at optimal, but not lower or higher, concentrations of glutaraldehyde. At 10 and 20 μL, the diameter was 0.18–1.50 μm and 0.20–1.30 μm, respectively; with most diameters less than 1.00 μm (**Figure 2A, B**). When glutaraldehyde was increased to 30 μL, the MSs exhibited a spheroid shape. The MS diameter was 0.30–2.20 μm, and 72.39% of the diameters were 0.40–1.10 μm, approximating a normal distribution (**Figure 2C, E**). However, when the crosslinker was increased to 40 μL, the diameter was 0.10–4.20 μm, and most diameters were greater than 1.50 μm (**Figure 2D**). Therefore, 30 μL of 25% glutaraldehyde was used for fabricating BSA- and PDGF-MSs. Three different amounts of BSA were used for encapsulation. When 1 mg BSA was used, MS molding was good. The diameter was 0.20–2.00 μm, approximating a normal distribution (**Figure 3A, A1, D**). As BSA increased, the diameter of the MSs increased as well (**Figure 3B, B1**). At 2 and 4 mg, the diameter was 1.10–1.80 μm and 0.20–2.80 μm, respectively. However, at 4 mg, the freeness of the MSs was reduced (**Figure 3C, C1**).

MS swelling index

The swelling index of the MSs encapsulated with the three different amounts of BSA increased markedly within the first 4 hours, and no significant difference was observed among the groups. At 4–10 hours, the increase in the swelling index was dramatically higher in the MSs group than in the BSA encapsulation group. At 10 hours, the swelling index tended to be stable, and water absorption reached saturation. Compared with the MSs group, the swelling index was lower in the three BSA encapsulation groups. As the amount of BSA increased, the swelling index decreased (**Figure 4**).

Encapsulation efficiency of MSs

In the 1 mg BSA-MSs group, the encapsulation efficiency of MSs for BSA was 79.52 ± 5.20%, and the encapsulation efficiency of MSs for PDGF-BB was 70.25 ± 2.22%.

Cumulative release curves for MSs

Cumulative release curves for BSA-MSs and PDGF-MSs over a period of 4 weeks is shown in **Figure 5**. In this period, except for the first day, BSA concentration in the leachate (supernatant) did not increase rapidly, but MSs continued to release BSA. Cumulative release gradually increased. Cumulative release of BSA by BSA-MSs was approximately 41.6 ± 5.0% at 1 week, 58.5 ± 5.6% at 2 weeks, 63.8 ± 5.0% at 3 weeks, and 69.0 ± 5.2% at 4 weeks. Cumulative release of PDGF by the PDGF-MSs was relatively lower than that of BSA by the BSA-MSs. From 1 to 4 weeks, the cumulative release values of PDGF-BB were 30.5 ± 3.9%, 39.1 ± 5.3%, 45.3 ± 5.2% and 52.0 ± 1.8%, respectively. Two-way analysis

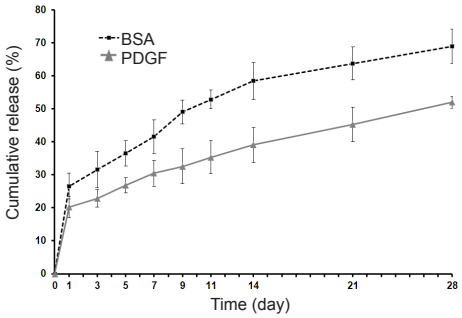

Figure 5 Sustained release curve of MSs.
Except for the first day, the concentration of BSA did not increase rapidly. Cumulative release of PDGF by PDGF-MSs was relatively lower than that of BSA by BSA-MSs. Two-way analysis of variance showed that the release rate of the BSA-MSs was greater than that of the PDGF-MSs ($P < 0.05$). However, there was no significant difference between the two groups in the tendency of the release rate to change with time ($P > 0.05$). All experiments were conducted six times. MSs: Microspheres; BSA: bovine serum albumin; PDGF: platelet-derived growth factor.

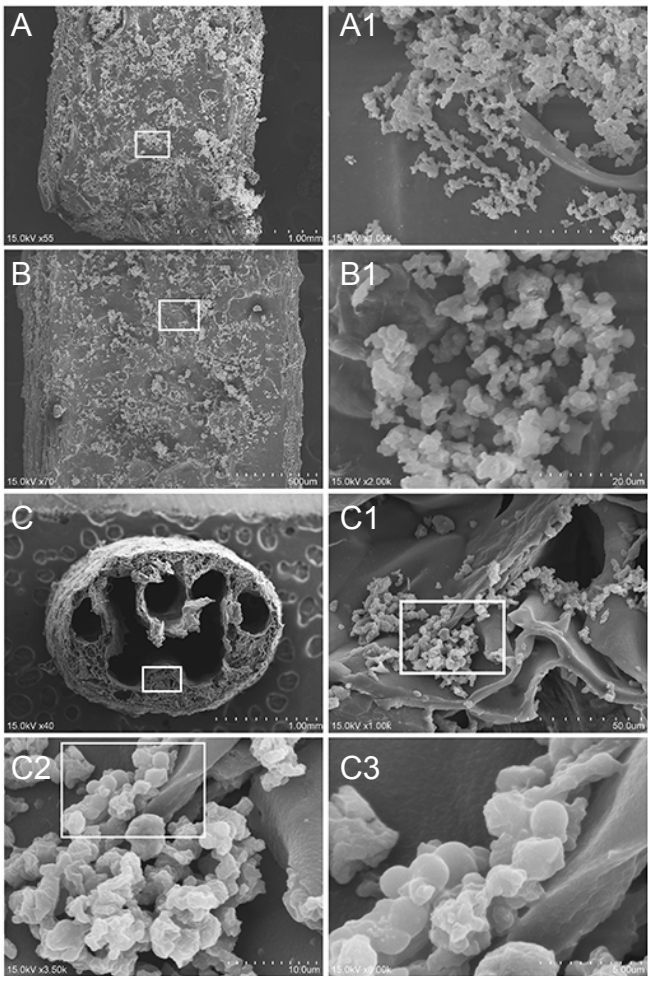

Figure 6 Scanning electron microscopy of MS/partition-type tubular scaffold or BSA-MS/partition-type tubular scaffold.
MSs or BSA-MSs were evenly distributed on the wall of the gray matter tube of the longitudinal section of the partition-type tubular scaffold. (A) Longitudinal section of MS/partition-type tubular scaffold; (B) longitudinal section of BSA-MS/partition-type tubular scaffold; (C) transverse section of BSA-MS/partition-type tubular scaffold. (A1, B1, C1, C2, C3) Magnified views of boxed areas in A, B, C, C1 and C2, respectively. Scale bars: 1.0 mm (A), 50 μm (A1), 50 μm (B), 20 μm (B1), 1.0 μm (C), 50 μm (C1), 10 μm (C2), 6.0 μm (C3). MSs: Microspheres; BSA: bovine serum albumin.

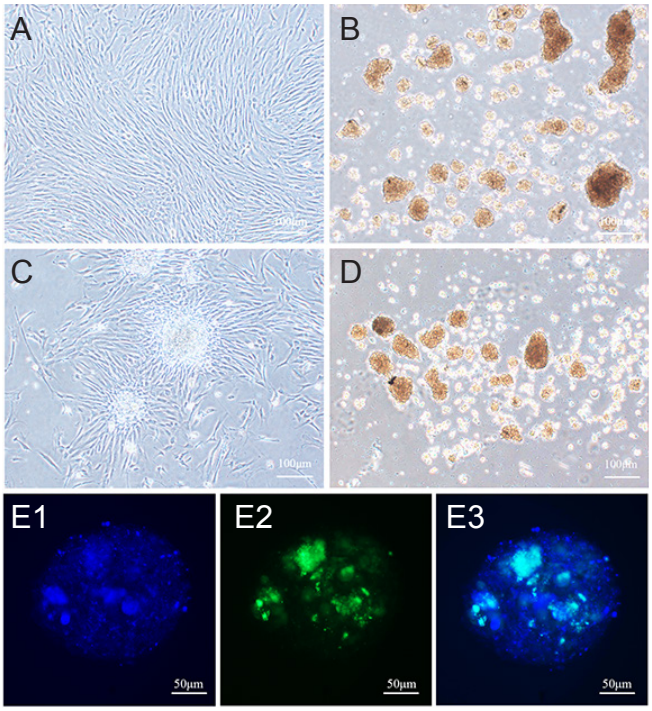

Figure 7 Neural progenitor cells induced from MUSE cells.
MUSE cells obtained from BMSCs formed large and translucent cell spheres in suspension culture or a single spindle-shaped cell in adhered culture. The cell spheres expressed the NPC marker DCX after 2–3 days of suspension culture with neural induction medium. (A) Growing BMSCs; (B) MUSE cells in suspension culture; (C) adherent MUSE cells; (D) MUSE-NPCs in suspension culture; (E1–E3) fluorescence staining of MUSE-NPCs for DCX. Scale bars: 10 μm (A–D) and 50 μm (E1–E3). BMSCs: Bone marrow stromal cells; MUSE-NPCs: neural progenitor cells differentiated *in vitro* from multilineage-differentiating stress-enduring cells.

of variance showed that the release rate of the BSA-MSs was greater than that of the PDGF-MSs ($P < 0.05$). However, there was no significant difference between the two groups in the tendency of the release rate to change with time ($P > 0.05$; **Figure 5**).

Observation of the MS/partition-type tubular scaffold

After the MS suspension was injected into the gray matter tube of the partition-type tubular scaffold, MSs were evenly distributed on the wall of the gray matter tube under the SEM (longitudinal section; **Figure 6A**). When BSA-MSs were similarly loaded, many BSA-MSs were distributed on the tube wall (**Figure 6B**), and some were found in small holes of the tube wall surface of the scaffold (**Figure 6C**).

MUSE-NPC harvesting

Human BMSCs were collected from adult bone marrow 4–7 days after treatment by density gradient centrifugation and the differential adhesion method (**Figure 7A**). Human BMSCs were treated with 0.25% trypsin-EDTA to obtain muse cells that could tolerate trypsinization. Large and translucent cellular spheres formed in suspension culture (**Figure 7B**). A single muse cell was spindle-shaped when adhered to the wall (**Figure 7C**). MUSE cells rapidly proliferated in alternating suspension–adhesion culture. At 2–3 days after

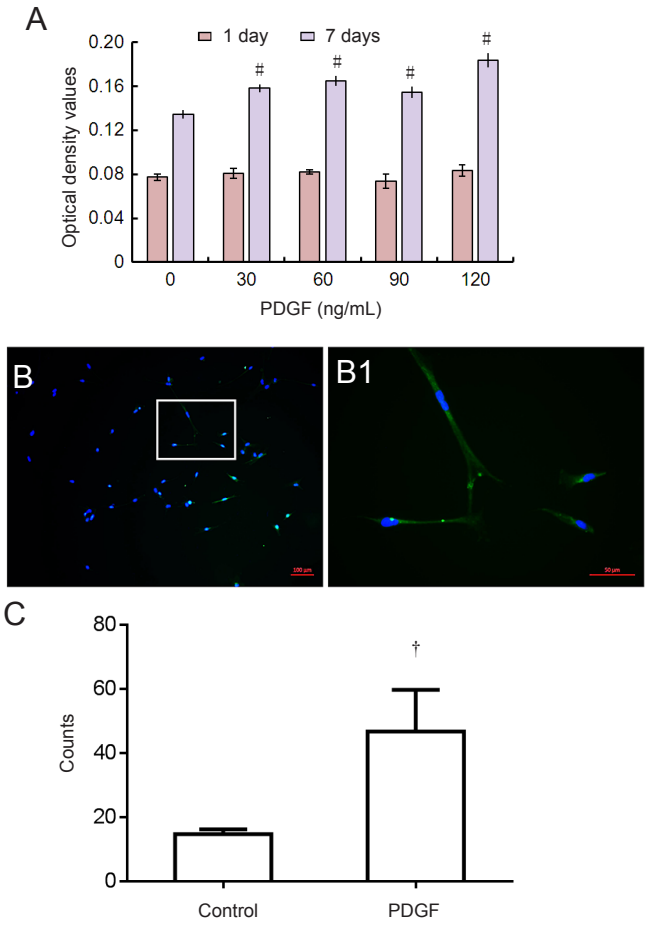

Figure 8 Effects of different concentrations of PDGF-BB on MUSE-NPCs.

(A) Effect of PDGF-BB on MUSE-NPC proliferation measured by CCK-8 assay. Cell proliferation was higher in the 120 ng/mL PDGF-BB group than in the other dosage groups. (B) Immunocytochemical staining showing the effect of PDGF-BB on MUSE-NPC differentiation (green fluorescence: MAP-2; blue fluorescence: DAPI); (B1) Magnified view of boxed area in B. (C) Effect of PDGF-BB on MUSE-NPC migration, indicating that PDGF-BB attracts MUSE-NPCs. Scale bars: 100 μm (B) or 50 μm (B1). The data were expressed as the mean ± SD (one-way analysis of variance followed by Dunnett's *post hoc* test). All experiments were conducted six times. PDGF: Platelet-derived growth factor; MUSE-NPCs: neural progenitor cells differentiated *in vitro* from multilineage-differentiating stress-enduring cells. #$P < 0.05$, *vs.* 1 day; †$P < 0.05$, *vs.* control.

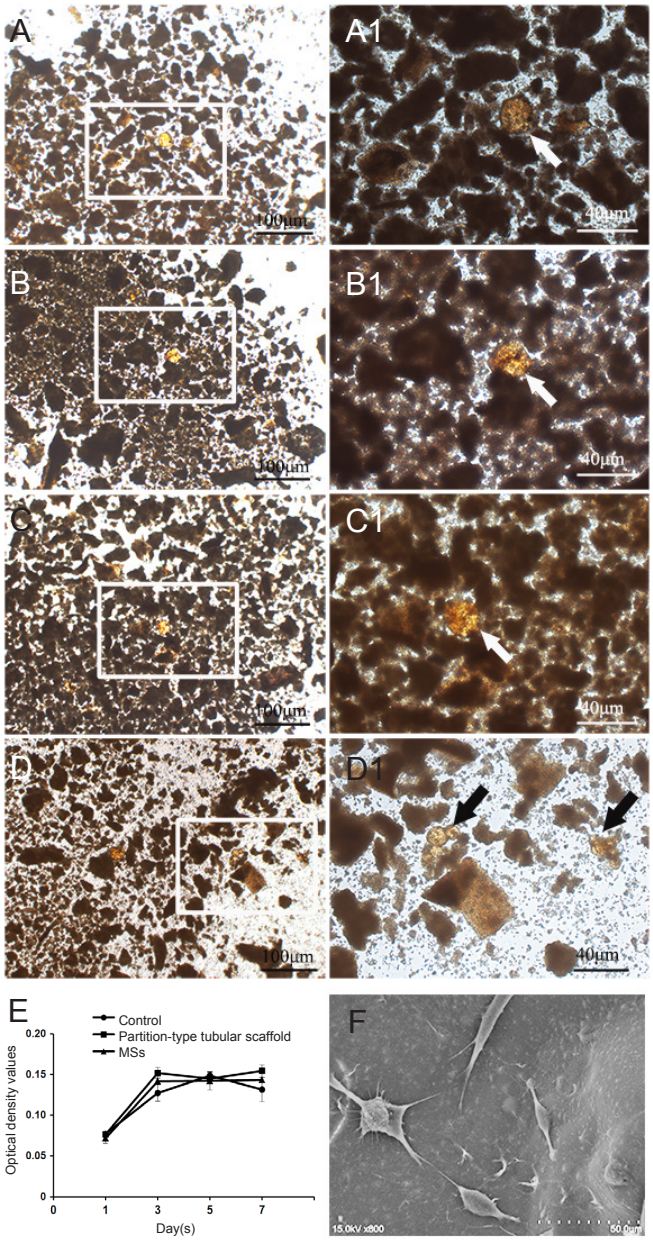

Figure 9 Effects of the MS/partition-type tubular scaffold on MUSE-NPC viability.

(A–D) Light microscopy of contact culture of MS/partition-type tubular scaffold with MUSE-NPCs for 1, 3, 5 and 7 days; (A1–D1) Magnified view of boxed areas in A–D. MUSE-NPCs grew well and formed cell spheres on the MS/partition-type tubular scaffold. (E) Effect of culture with MSs or partition-type tubular scaffold leachate on MUSE-NPC viability. Two-way analysis of variance and analysis of cell viability showed that there were no significant differences among the groups ($P > 0.05$), suggesting that the partition-type tubular scaffold and MSs do not affect the growth of MUSE-NPCs. (F) Scanning electron microscopy for MUSE-NPC growth in the PDGF-MS/partition-type tubular scaffold. The arrows indicate MUSE-NPC spheres. Scale bar: 100 μm (A–D), 40 μm (A1–D1) and 50 μm (F). All experiments were conducted six times. PDGF: Platelet-derived growth factor; MUSE-NPCs: neural progenitor cells differentiated in vitro from multilineage-differentiating stress-enduring cells.

culture with neural induction medium, the suspended single cells quickly aggregated to form translucent and well-defined cellular spheres (**Figure 7D**). Immunocytochemical staining revealed that the multicellular spheres expressed the NPC marker DCX (**Figure 7E1–3**).

Effects of PDGF-BB on MUSE-NPCs

Effect of PDGF-BB on MUSE-NPC growth

After a 1-week treatment with PDGF-BB, MUSE-NPCs proliferated. These cells grew well and were dense in the 120 ng/mL group. CCK-8 assay demonstrated that compared with the control group, MUSE-NPCs proliferation significantly increased in the PDGF-BB group. The cell proliferation was higher in the 120 ng/mL PDGF-BB group than in other dos-

age groups ($P < 0.05$). Moreover, no significant difference was determined among the other dosage groups (**Figure 8A**).

After 1-week culture with 120 ng/mL PDGF-BB neural induction medium, immunocytochemical staining showed that most cells expressed the neuronal marker MAP-2, and the cells began to extend slender processes and branches that resembled neurites (**Figure 8B**).

Effect of PDGF-BB on MUSE-NPC migration

Crystal violet staining showed that in the PDGF-BB group, MUSE-NPCs had migrated to the lower chamber of the Transwell. The number of cells in the lower chamber was 46.7 ± 13.0 cells/field. In the control group, the number of cells in the lower chamber was 14.7 ± 1.5 cells/field. Significant differences in the number of cells in the lower chamber were found between the two groups ($P < 0.05$), indicating that PDGF-BB is chemoattractive for MUSE-NPCs (**Figure 8C**).

Effects of the MS/partition-type tubular scaffold on MUSE-NPCs

Effect of the MS/partition-type tubular scaffold on MUSE-NPC contact growth

After contact culture of MUSE-NPCs with the MSs and partition-type tubular scaffold for 1, 3, 5 and 7 days, MUSE-NPCs grew well and formed cellular spheres. The scattered cell bodies were translucent (**Figure 9A–D**). The results suggest that direct contact of the MS/partition-type tubular scaffold with MUSE-NPCs does not impact cell growth, with good biocompatibility.

MUSE-NPC viability

After MUSE-NPCs were separately cultured with leachate containing MSs and the partition-type tubular scaffold for 1, 3, 5 and 7 days, MUSE-NPC viability was assessed with the CCK-8 assay. Compared with the control group (neural induction medium alone), no significant difference in cell viability was found at the various time points in any group ($P > 0.05$), suggesting that the partition-type tubular scaffold and MSs do not affect the growth of MUSE-NPCs (**Figure 9E**).

Effect of the PDGF-MS/partition-type tubular scaffold on MUSE-NPC contact growth

By SEM, after 1 month of contact culture, MUSE-NPCs were still attached to the inner cavity of the partition-type tubular scaffold. The cell bodies were spindle shaped, had many processes, and grew well (**Figure 9F**).

Discussion

Chitin, the most easily obtained polysaccharide polymer in nature, has good biocompatibility. Chitin is deacetylated to form chitosan, which also has excellent biocompatibility and biodegradability. The intermediate degradation product, chitooligosaccharide, promotes neural regeneration (Yang et al., 2009; Jin et al., 2016). The final degradation products, carbon dioxide and water, are directly discharged from the body (Skop et al., 2013; Fang et al., 2014).

Chitin and chitosan have been widely used clinically in nervous system repair, especially in tissue engineering as a scaffold material (Rodríguez-Vázquez et al., 2015). We also used chitosan for the preparation of the partition-type tubular scaffold. Many studies have used chitosan to produce MSs (Wu et al., 2014; Sivashankari and Prabaharan, 2016). In our tissue engineering, the same material was used to avoid possible interactions and adverse reactions of different materials in vivo. The MUSE-NPCs, which were cultured with the partition-type tubular scaffold and MS leachate or the MS/partition-type tubular scaffold through direct contact, grew well, indicating good biocompatibility.

As in our previous study (Wang et al., 2013), gelatin was added to improve the plasticity and toughness of the partition-type tubular scaffold. The sample scaffold was pre-frozen at −20°C for various time periods, frozen, and dried at −40°C and 0.02 Pa. We found that when the pre-freezing time was 2 hours, the molding rate significantly increased, reaching approximately 69.0%, but the porosity was still low. However, the partition-type tubular scaffold contained regenerative channels for gray matter and the main descending bundle (corticospinal and rubrospinal tracts) that controls limb movement, with thin tube walls. A previous study showed that greater than 70% porosity supported the growth of axons into the pores within two weeks. However, if the pores were not optimal, the axons were hindered. The porosity was inversely proportional to the strength of the material after molding, and therefore we did not increase the porosity of the tube wall. If strength is not compromised, a good perforated pore structure can be considered. This allows axons to extend (Kubinová and Syková, 2012; Vigani, 2017) and promotes the formation of blood vessels and a vascular network (Dadsetan et al., 2008).

In tissue engineering, seed cells are mainly used to complement the tissue cells that have been lost at the site of injury, improve the microenvironment through a secretory effect, and promote tissue regeneration (Georgiou et al., 2015). However, these cells can promote regeneration only if they remain at the transplant site. Chemokines that guide cell migration may be an ideal option to help retain seed cells in a certain area. Many studies have reported that PDGF-BB has a chemotactic effect on BMSCs. PDGF-BB is the major chemoattractant that guides MSCs into injured areas (Deuel et al., 1991; Heldin et al., 1999; Tyurin-Kuzmin et al., 2016). In this study, the Transwell assay revealed that PDGF-BB also has a chemoattractive effect on MUSE-NPCs. However, only a sufficient concentration of PDGF-BB in the scaffold can persistently attract and retain MUSE-NPCs. Accordingly, we used polymer-based MSs, which have been widely used to control the release of protein/peptide drugs. MSs are mainly composed of natural polymers, such as chitosan, agarose and alginate, and synthetic polymers, such as polyglycolic acid and polycaprolactone (Ma, 2014; Rambhia et al., 2015). NGF-delivering chitosan MSs have been reported to promote repair following peripheral nerve injury (Zeng et al., 2011, 2014). PDGF-MSs appear to promote angiogenesis at the site of injury (Choi et al., 2013; Subbiah et al., 2015), the differentiation of seed cells, and the regeneration of skin and

bone (Jiang et al., 2013; Mohan et al., 2017). The fabrication of chitosan-based MSs for sustained release of PDGF in the present study represents a novel approach for neural repair.

During the preparation of chitosan MSs, chemical or ionic crosslinking is commonly used (Sivashankari and Prabaharan, 2016). Jiang et al. (2014) used glutaraldehyde crosslinking for TGF-β3-MSs and obtained good results, and therefore we also used this molding method. Four concentrations of glutaraldehyde were used, and the diameter of the MSs ranged from 0.20 to 4.20 μm. In the 30 μL crosslinker group, the diameter of 72.39% of the MSs ranged from 0.40 to 1.10 μm, approximating a normal distribution. Therefore, 30 μL 25% glutaraldehyde was selected for preparing MSs. Under the SEM, in the 1 mg BSA-MSs group, MSs were regularly spherical, and the diameter ranged from 0.20 to 2.00 μm. The encapsulation efficiency was (72.33 ± 1.28)%. The swelling index of the MSs gradually decreased. This is probably because when the amount of BSA encapsulated on the surface of MSs increases, there is reduced room for water absorption. Ideal MSs for protein drug delivery should minimize the burst release effect and provide sustained and long-term release. Moreover, protein binding to and release from MSs must not impact biological activity. Therefore, spatiotemporal control of the release of protein drugs that directly or indirectly affect cellular signaling or tissue regeneration is needed (Rambhia and Ma, 2015). In the present study, there was no explosive release of BSA or PDGF by the MSs. Over a period of 4 weeks, BSA and PDGF were steadily released. Cumulative release by the BSA-MSs and PDGF-MSs was 69.0% and 52.0%, respectively. Compared with other studies, our cumulative release was relatively low. The reasons for this difference may include the following: (1) the polymer materials used to prepare the MSs differed; and (2) the PDGF-BB amounts used to prepare the PDGF-MSs were often larger in these other studies (*i.e.*, 25 and 300 μg/mL) (Wu et al., 2016; Mohan et al., 2017). Compared with chitosan MSs loaded with other types of cytokines at similar or higher amounts, the cumulative release was similar, or even sustained for a longer period (Zeng et al., 2011, 2014; Jiang et al., 2014).

BMSCs are isolated from adult bone marrow, and then used to screen for MUSE cells. The NPC marker DCX was induced by neural induction medium, indicating that MUSE-NPCs were obtained (Farzanehfar et al. 2017). Immunocytochemical staining showed that PDGF-BB not only promotes MUSE-NPC growth in the PDGF-MS/partition-type tubular scaffold but also induces the extension of neuritic processes and expression of the neuronal marker MAP-2. Further study is needed to full elucidate the effects of PDGF-BB on the growth and differentiation of MUSE-NPCs.

To summarize, we fabricated, for the first time, chitosan-based microspheres that allow sustained release of PDGF-BB by optimization of the cross-linking procedure. Furthermore, we fabricated partition-type tubular scaffolds with an optimal pre-freezing protocol, and we then loaded these with PDGF-releasing microspheres. The PDGF-MS-containing tubular scaffolds exhibited suitable biocompatibility towards MUSE-NPCs and could promote the directional migration and growth of these cells. Collectively, our findings suggest that a combination of a partition-type tubular scaffold, PDGF-MSs and MUSE-NPCs may have therapeutic potential for spinal cord injuries.

Acknowledgments: *We would like to thank Ya-Ping Zhang for providing technical support.*
Author contributions: *XC designed the study and analyzed data. MLX performed experiments. CNW, LZZ, YHZ, CLZ and JW provided technical support. YC analyzed data. YMY provided material and technical support. XDW designed the study and wrote the manuscript. All authors approved the final version of the paper.*
Conflicts of interest: *The authors declare that there is no duality of interest associated with this manuscript.*
Financial support: *This study was supported by the Natural Science Foundation of China, No. 81501610, 81350030; the Priority Academic Program Development of Jiangsu Higher Education Institutes of China. Funders had no involvement in the study design; data collection, analysis, and interpretation; paper writing; or decision to submit the paper for publication.*
Institutional review board statement: *The procedures were approved by the Ethics Committee of Affiliated Hospital of Nantong University of China (approval No. 2015-052).*
Copyright license agreement: *The Copyright License Agreement has been signed by all authors before publication.*
Data sharing statement: *Datasets analyzed during the current study are available from the corresponding author on reasonable request.*
Plagiarism check: *Checked twice by iThenticate.*
Peer review: *Externally peer reviewed.*
Open access statement: *This is an open access journal, and articles are distributed under the terms of the Creative Commons Attribution-Non-Commercial-ShareAlike 4.0 License, which allows others to remix, tweak, and build upon the work non-commercially, as long as appropriate credit is given and the new creations are licensed under the identical terms.*
Open peer reviewer: *Jian-Xun Ding, Chang Chun Institute of Applied Chemistry Chinese Academy of Sciences, Key Laboratory of Polymer Ecomaterials, China.*
Additional file: *Open peer review report 1.*

References

Agbay A, Edgar JM, Robinson M, Styan T, Wilson K, Schroll J, Ko J, Khadem Mohtaram N, Jun MB, Willerth SM (2016) Biomaterial strategies for delivering stem cells as a treatment for spinal cord injury. Cells Tissues Organs 202:42-51.

Ahuja CS, Wilson JR, Nori S, Kotter MRN, Druschel C, Curt A, Fehlings MG (2017) Traumatic spinal cord injury. Nat Rev Dis Primers 27:17018.

Assinck P, Duncan GJ, Hilton BJ, Plemel JR, Tetzlaff W (2017) Cell transplantation therapy for spinal cord injury. Nat Neurosci 20:637-647.

Badner A, Siddiqui AM, Fehlings MG (2017) Spinal cord injuries: how could cell therapy help? Expert Opin Biol Ther 17:529-41.

Bellamkonda RV (2006) Peripheral nerve regeneration: an opinion on channels, scaffolds and anisotropy. Biomaterials 27:3515-3518.

Bryant SJ, Cuy JL, Hauch KD, Ratner BD (2007) Photo-patterning of porous hydrogels for tissue engineering. Biomaterials 28:2978-2986.

Choi DH, Subbiah R, Kim IH, Han DK, Park K (2013) Dual growth factor delivery using biocompatible core-shell microcapsules for angiogenesis. Small 9:3468-3476.

Dadsetan M, Hefferan TE, Szatkowski JP, Mishra PK, Macura SI, Lu L, Yaszem-ski MJ (2008) Effect of hydrogel porosity on marrow stromal cell phenotypic expression. Biomaterials 29:2193-2202.

Deuel TF, Kawahara RS, Mustoe TA, Pierce AF (1991) Growth factors and wound healing: platelet-derived growth factor as a model cytokine. Annu Rev Med 42:567-584.

Fang J, Zhang Y, Yan S, Liu Z, He S, Cui L, Yin J (2014) Poly (L-glutamic acid)/chitosan polyelectrolyte complex porous microspheres as cell microcarriers for cartilage regeneration. Acta Biomater 10:276-288.

Farzanehfar P, Lu SS, Dey A, Musiienko D, Baagil H, Horne MK, Aumann TD (2017) Evidence of functional duplicity of Nestin expression in the adult mouse midbrain. Stem Cell Res 19:82-93.

Georgiou M, Golding J P, Loughlin A J, Kingham PJ, Phillips JB (2015) Engineered neural tissue with aligned, differentiated adipose-derived stem cells promotes peripheral nerve regeneration across a critical sized defect in rat sciatic nerve. Biomaterials 37:242-251.

Heldin CH, Westermark B (1999) Mechanism of action and in vivo role of platelet-derived growth factor. Physiol Rev 79:1283-1316.

Hoffman AM, Dow SW (2016) Concise review: stem cell trials using companion animal disease models. Stem Cells 34:1709-1729.

Hong JY, Lee SH, Lee SC, Kim JW, Kim KP, Kim SM, Tapia N, Lim KT, Kim J, Ahn HS, Ko K, Shin CY, Lee HT, Schöler HR, Hyun JK, Han DW (2014) Therapeutic potential of induced neural stem cells for spinal cord injury. J Biol Chem 289:32512-32525.

Jia H, Wang Y, Tong X J, Liu GB, Li Q, Zhang LX, Sun XH (2012) Sciatic nerve repair by acellular nerve xenografts implanted with BMSCs in rats xenograft combined with BMSCs. Synapse 66:256-269.

Jiang B, Zhang G, Brey EM (2013) Dual delivery of chlorhexidine and platelet-derived growth factor-BB for enhanced wound healing and infection control. Acta Biomater 9:4976-4984.

Jiang K, Wang Z, Du Q, Yu J, Wang A, Xiong Y (2014) A new TGF-β3 controlled-released chitosan scaffold for tissue engineering synovial sheath. J Biomed Mater Res A 102:801-807.

Jin X, Yamashita T (2016) Microglia in central nervous system repair after injury. J Biochem 159:491-496.

Kawabata S, Takano M, Numasawa-Kuroiwa Y, Itakura G, Kobayashi Y, Nishiyama Y, Sugai K, Nishimura S, Iwai H, Isoda M, Shibata S, Kohyama J, Iwanami A, Toyama Y, Matsumoto M, Nakamura M, Okano H (2016) Grafted human ips cell-derived oligodendrocyte precursor cells contribute to robust remyelination of demyelinated axons after spinal cord injury. Stem Cell Rep 6:1-8.

Kim MS, Lee HB (2014) Perspectives on tissue-engineered nerve regeneration for the treatment of spinal cord injury. Tissue Eng Part A 20:1781-1783.

Kornhaber R, Mclean L, Betihavas V, Cleary M (2018) Resilience and the rehabilitation of adult spinal cord injury survivors: a qualitative systematic review. J Adv Nurs 74:23-33.

Kubinová S, Syková E (2012) Biomaterials combined with cell therapy for treatment of spinal cord injury. Regen Med 7:207-224.

Kuroda Y, Kitada M, Wakao S, Nishikawa K, Tanimura Y, Makinoshima H, Goda M, Akashi H, Inutsuka A, Niwa A, Shigemoto T, Nabeshima Y, Nakahata T, Nabeshima Y, Fujiyoshi Y, Dezawa M (2010) Unique multipotent cells in adult human mesenchymal cell populations. Proc Natl Acad Sci U S A 107:8639-8643.

Lu P, Woodruff G, Wang Y, Graham L, Hunt M, Wu D, Boehle E, Ahmad R, Poplawski G, Brock J, Goldstein L, Tuszynski MH (2014) Long-distance axonal growth from human induced pluripotent stem cells after spinal cord injury. Neuron 83:789-796.

Ma GH (2014) Microencapsulation of protein drugs for drug delivery: strategy, preparation, and applications. J Control Release 193:324-340.

Madigan NN, McMahon S, O'Brien T, Yaszemski MJ, Windebank AJ (2009) Current tissue engineering and novel therapeutic approaches to axonal regeneration following spinal cord injury using polymer scaffolds. Respir Physiol Neurobiol 169:183-199.

Mohan S, Raghavendran HB, Karunanithi P, Murali MR, Naveen SV, Talebian S, Mehrali M, Mehrali M, Natarajan E, Chan CK, Kamarul T (2017) Incorporation of human-platelet-derived growth factor-BB encapsulated poly (lactic-co-glycolicacid) microspheres into 3D CORAGRAF enhances osteogenic differentiation of mesenchymal stromal cells. ACS Appl Mater Interfaces 9:9291-9303.

Mohtaram NK, Montgomery A, Willerth SM (2013) Biomaterial-based drug delivery systems for the controlled release of neurotrophic factors. Biomed Mater 8:022001.

Muheremu A, Peng J, Ao Q (2016) Stem cell based therapies for spinal cord injury. Tissue Cell 48:328-333.

Nagoshi N, Okano H (2017) Applications of induced pluripotent stem cell technologies in spinal cord injury. J Neurochem 141:848-860.

Pascual-Gil S, Simón-Yarza T, Garbayo E, Prosper F, Blanco-Prieto MJ (2015) Tracking the in vivo release of bioactive NRG from PLGA and PEG-PLGA microparticles in infarcted hearts. J Control Release 220:388-396.

xPitorre M, Gondé H, Haury C, Messous M, Poilane J, Boudaud D, Kanber E, Rossemond Ndombina GA, Benoit JP, Bastiat G (2017) Recent advances in nanocarrier-loaded gels: which drug delivery technologies against which diseases? J Control Release 266:140-155.

Ponte AL, Marais E, Gallay N, Domenech J (2007) The in vitro migration capacity of human bone marrow mesenchymal stem cells: comparison of chemokine and growth factor chemotactic activities. Stem Cells 25:1737-1745.

Rambhia KJ, Ma PX (2015) Controlled drug release for tissue engineering. J Control Release 219:119-128.

Rodríguez-Vázquez M, Vega-Ruiz B, Ramos-Zúñiga R, Saldaña-Koppel DA, Quiñones-Olvera LF (2015) Chitosan and its potential use as a scaffold for tissue engineering in regenerative medicine. Biomed Res Int 2015:821279.

Sivashankari PR, Prabaharan M (2016) Prospects of chitosan-based scaffolds for growth factor release in tissue engineering. Int J Biol Macromol 93:1382-1389.

Skop NB, Calderon F, Levison SW, Gandhi CD, Cho CH (2013) Heparin crosslinked chitosan microspheres for the delivery of neural stem cells and growth factors for central nervous system repair. Acta Biomater 9:6834-6843.

Subbiah R, Hwang MP, Van SY, Do SH, Park H, Lee K, Kim SH, Yun K, Park K (2015) Osteogenic/angiogenic dual growth factor delivery microcapsules for regeneration of vascularized bone tissue. Adv Healthc Mater 4:1982-1992.

Tetzlaff W, Okon EB, Karimi-Abdolrezaee S, Hill CE, Sparling JS, Plemel JR, Plunet WT, Tsai EC, Baptiste D, Smithson LJ, Kawaja MD, Fehlings MG, Kwon BK (2011) A systematic review of cellular transplantation therapies for spinal cord injury. J Neurotrauma 28:1611-1682.

Tyurin-Kuzmin PA, Zhdanovskaya ND, Sukhova AA, Sagaradze GD, Albert EA, Ageeva LV, Sharonov GV, Vorotnikov AV, Tkachuk VA (2016) Nox4 and Duox1/2 mediate Redox activation of mesenchymal cell migration by PDGF. PLoS One 11:e0154157.

Wang LL, Zhang CL (2018) Engineering new neurons: in vivo reprogramming in mammalian brain and spinal cord. Cell Tissue Res 371:201-212.

Wang X, Ma M, Wu Y, Niu X, Zhang Y, Wang X, Chen X (2016) Study on induction of human muse cells into neural precursor cells in vitro. Chin J Biomed Eng 35:218-224.

Wang XS, Li Y, Gao YF, Chen X, Yao J, Lin WW, Chen Y, Liu J, Yang YM, Wang XD (2013) Combined use of spinal cord-mimicking partition type scaffold architecture and neurotrophin-3 for surgical repair of completely transected spinal cord in rats. J Biomat Sci-Polym E 24:927-939.

Wright KT, El Masri W, Osman A, Chowdhury J, Johnson WE (2011) Concise review: Bone marrow for the treatment of spinal cord injury: mechanisms and clinical applications. Stem Cells 29:169-178.

Wu H, Liu J, Wu J, Wan Y, Chen Y (2016) Controlled delivery of platelet-derived growth factor-BB from injectable microsphere/hydrogel-composites. Colloids Surf B Biointerfaces 148:308-316.

Wu H, Xu Y, Liu G, Ling J, Dash BC, Ruan J, Zhang C (2014) Emulsion cross-linked chitosan/nanohydroxyapatite microspheres for controlled release of alendronate. J Mater Sci Mater Med 25:2649-2658.

Vigani B, Rossi S, Sandri G, Bonferoni MC, Ferrari F (2017) Design and criteria of electrospun fibrous scaffolds for the treatment of spinal cord injury. Neural Regen Res 12:1786-1790.

Yang Y, Liu M, Gu Y, Lin S, Ding F, Gu X (2009) Effect of chitooligosaccharide on neuronal differentiation of PC-12 cells. Cell Biol Int 33:352-356.

Yun S, Huang JJ (2016) Routes for drug delivery: sustained-release devices. Dev Ophthalmol 55:84-92.

Zeng W, Rong M, Hu X, Xiao W, Qi F, Huang J, Luo Z (2014) Incorporation of chitosan microspheres into collagen chitosan scaffolds for the controlled release of nerve growth factor. PLoS One 9:e101300.

Zeng W, Huang J, Hu X, Xiao W, Rong M, Yuan Z, Luo Z (2011) Ionically cross-linked chitosan microspheres for controlled release of bioactive nerve growth factor. Int J Pharm 421:283-290.

Zhang W, Zhu XQ, Zhang DC (2016) Transplantation of bone marrow mesenchymal stem cells overexpressing Shootin1 for treatment of spinal cord injury. Zhongguo Zuzhi Gongcheng Yanjiu 20:7507-7517.

(*Copyedited by Patel B, Robens J, Wang J, Li CH, Qiu Y, Song LP, Zhao M*)